Light curves of ten Centaurs from K2 measurements

Gábor Marton [a,*], Csaba Kiss [a], László Molnár [a,b], András Pál [a], Anikó Farkas-Takács [a,e],
Gyula M. Szabó [c,d], Thomas Müller [f], Victor Ali-Lagoa [f], Róbert Szabó [a,b], József Vinkó [a],
Krisztián Sárneczky [a], Csilla E. Kalup [a,e], Anna Marciniak [g], Rene Duffard [h], László L. Kiss [a,i]

[a] Konkoly Observatory, Research Centre for Astronomy and Earth Sciences, Konkoly Thege 15-17, H-1121 Budapest, Hungary
[b] MTA CSFK Lendület Near-Field Cosmology Research Group, Konkoly Thege 15-17, H-1121 Budapest, Hungary
[c] ELTE Gothard Astrophysical Observatory, H-9704 Szombathely, Szent Imre herceg út 112, Hungary
[d] MTA-ELTE Exoplanet Research Group, H-9704 Szombathely, Szent Imre herceg út 112, Hungary
[e] Eötvös Loránd University, Faculty of Science, Pázmány P. st. 1/A, 1171 Budapest, Hungary
[f] Max-Planck-Institut für extraterrestrische Physik, Giessenbachstrasse, Garching, Germany
[g] Astronomical Observatory Institute, Faculty of Physics, A. Mickiewicz University, Słoneczna 36, 60-286 Poznań, Poland
[h] Instituto de Astrofísica de Andalucía (CSIC), Glorieta de la Astronomía s/n, 18008 Granada, Spain
[i] Sydney Institute for Astronomy, School of Physics A28, University of Sydney, NSW 2006, Australia

ARTICLE INFO

ABSTRACT

Here we present the results of visible range light curve observations of ten Centaurs using the *Kepler* Space Telescope in the framework of the K2 mission. Well defined periodic light curves are obtained in six cases allowing us to derive rotational periods, a notable increase in the number of Centaurs with known rotational properties.

The low amplitude light curves of (471931) 2013 PH_{44} and (250112) 2002 KY_{14} can be explained either by albedo variegations, binarity or elongated shape. (353222) 2009 YD_7 and (514312) 2016 AE_{193} could be rotating elongated objects, while 2017 CX_{33} and 2012 VU_{85} are the most promising binary candidates due to their slow rotations and higher light curve amplitudes. (463368) 2012 VU_{85} has the longest rotation period, P = 56.2 h observed among Centaurs. The P > 20 h rotation periods obtained for the two potential binaries underlines the importance of long, uninterrupted time series photometry of solar system targets that can suitably be performed only from spacecraft, like the *Kepler* in the K2 mission, and the currently running TESS mission.

1. Introduction

Centaurs are small solar system objects on non-resonant, giant planet crossing orbits (Gladman et al., 2008), which leads to frequent encounters with the giant planets and results in short dynamical lifetimes. Their origin is the Kuiper belt or the scattering disk, forming a bridge between the transneptunian objects (TNOs) and Jupiter–family comets (Tiscareno and Malhotra, 2003; Di Sisto and Brunini, 2007; Bailey and Malhotra, 2009). Due to their relative proximity they provide an insight into the properties of outer solar system objects at the size scale of ~10–100 km (Duffard et al., 2014), which is currently unaccessible in the more distant transneptunian region by typical ground-based observations. Light curve observations and accurate determination of rotational periods of Centaurs are rare. In the recent review by Peixinho et al. (2020) there are 20 Centaurs with reliable light curve properties.

In several cases brightness variations were reported, but no definite

---

* Corresponding author.
E-mail address: marton.gabor@csfk.mta.hu (G. Marton).

periods could be derived, e.g. in the case of 2010 RF$_{43}$ or 2010 TY$_{53}$ (Benecchi and Sheppard, 2013); or (148975) 2001 XA$_{225}$ and (315898) 2008 QD$_4$ (Hromakina et al., 2018). This could be due to a common effect of low light curve amplitudes and the faintness of the targets, and/ or due to rotation periods longer that could be deduced from typical ground-based observations due to the limited length of the observing blocks.

As described in Peixinho et al. (2020) Centaurs typically rotate faster than transneptunian objects (mean rotation periods of 8.1 h and 8.45 h, respectively, Peixinho et al., 2020; Thirouin and Sheppard, 2019) and they do not show the correlation between light curve amplitude and absolute magnitude observed among transneptunian objects (Duffard et al., 2009; Benecchi and Sheppard, 2013), which might be explained by the different collisional evolution of small and large transneptunian objects (Davis and Farinella, 1997).

Periodic light curve variations of a single body can be due to elongated shape or albedo variegations on the surface, or the combination of the two. For minor planets, below the dwarf planet size limit (radius of ~200–300 km, Lineweaver and Norman, 2017), light curve variation in most cases is explained by shape effects. Binaries can be identified with high probability from light curves only in those special cases when we see a contact binary system under a sufficiently high aspect angle, and binarity is confirmed by multiple epoch observations (Lacerda and Jewitt, 2007). Light curves due to a deformed shape are often interpreted through equilibrium states of a strengthless body ('rubble-pile') in which case the shape is a Jacobi ellipsoid with a well-defined rotation period for a specific density. This equilibrium density is rather a lower limit for a real object with non-zero internal strength. A rotation period notably shorter than the equilibrium value (typically P $\gtrsim$ 1 d, see a detailed discussion in Section 4.2) can be interpreted as an indication of a binary system (Leone et al., 1984; Thirouin et al., 2010; Benecchi and Sheppard, 2013).

There are only two binary Centaurs identified so far: (65489) Ceto-Phorcys and (42355) Typhon-Echidna, both through direct imaging. We have to note here that there is some ambiguity in the definition of the Centaurs as a dynamical class. According to the historical definition Centaurs are objects in the giant planet realm whose evolution is currently not controlled by Jupiter (see the discussion in Gladman et al., 2008). A simple definition is that the semi-major axes of their orbits are between that of Jupiter and Neptune. The Gladman et al. (2008) dynamical classification scheme uses an additional criterion that a Centaur has to have a perihelion distance q > 7.35 AU and a Tisserand parameter of T$_J$ > 3.05 to distinguish these objects from Jupiter family comets. In this scheme e.g. (60558) Echeclus (q = 5.8 AU, T$_J$ = 3.03) and (52782) Okyrhoe (q = 5.8 AU, T$_J$ = 2.95), which are traditionally considered as Centaurs, are classified as 'Jupiter coupled'. The two binaries mentioned above, Ceto-Phorcys and Typhon-Echidna, are classified as Centaurs by the Deep Ecliptic Survey (Elliot et al., 2005), but are considered as scattered disk objects according to Gladman et al. (2008). We consider them here as these are the only known binaries which are at least dynamically close to the Centaur group, and they are also listed in the recent review of Centaurs by Peixinho et al. (2020).

Dotto et al. (2008) found a rotation period of 4.43 ± 0.03 h and a light curve amplitude of 0.13 ± 0.02 mag for Ceto-Phorcys. This is an unexpected result, as according to Grundy et al. (2007) this is a tidally evolved and spin locked binary system, with a small orbital eccentricity (e ≤0.013) and orbital period of P = 9.554 d. The Typhon-Echidna system is the other known binary Centaur, discovered by Noll et al. (2006), with an orbital period of P$_{orb}$ = 18^d.98 and semi-major axis of a = 1629 km (Grundy et al., 2008). In contrast to Ceto-Phorcys the binary orbit of Typhon-Echidna is rather eccentric (e = 0.53), showing that this is not a tidally evolved system. Thirouin et al. (2010) obtained a tentative rotation period of P$_{rot}$ = 9.67 h and a small light curve amplitude of Δm = 0^m.98 ± 0^m.01, consistent with other studies reporting on nearly flat light curves (Ortiz et al., 2003; Sheppard and Jewitt, 2003).

A large fraction of binaries originally in high eccentricity orbits can evolve to circular and very tight orbits due to Kozai effects (Porter and Grundy, 2012). An originally triple system that loses a component will also end up in a very tight pair (Margot et al., 2015). The angular resolution of the Hubble Space Telescope – that has detected most of the known transneptunian and Centaur binaries – allows the detection of a nearly equal brightness binary with a semi-major axis of ~400 km at 10 AU (typical perihelion distance of Centaurs); proportionally wider systems can be discovered at larger heliocentric distances. Due to the lack of suitable spatial resolution more compact systems can typically be discovered through the detection of their characteristic light curves, i.e. large, Δm $\gtrsim$1 mag amplitudes with U-shaped maxima and V-shaped minima (see e.g. Thirouin and Sheppard, 2018, for a discussion of contact binary systems in the plutino population). In some rare cases binary nature can be deduced from stellar occultation observations, as in the case of 2014 MU$_{69}$ (Moore et al., 2018).

As suggested by Thirouin and Sheppard (2018), nearly half of the plutino population may be contact or a tight binary system. Since plutinos are thought to be one of the parent populations of Centaurs (Di Sisto et al., 2010), one can expect a similar abundance of contact and tight binaries in the Centaur population, too, assuming that tight systems remains intact in giant planet encounters.

Studies of a large sample of minor planet light curves observed in the framework of the K2 mission of the *Kepler* Space Telescope (Howell et al., 2014) showed an overabundance of long (up to several days) rotation periods among main-belt asteroids (Szabó et al., 2016; Molnár et al., 2018). In the case of Jovian Trojans a binary fraction of 6–36% (Ryan et al., 2017) and ~20% (Szabó et al., 2017) was estimated from the data. These studies were carried out in the course of systematic programs in the K2 mission, aimed at obtaining light curves of solar system targets, including main belt asteroids (Szabó et al., 2015, 2016; Berthier et al., 2016; Molnár et al., 2018), Jovian Trojans (Ryan et al., 2017; Szabó et al., 2017), transneptunian objects (Pál et al., 2015a, 2015b, 2016; Benecchi et al., 2018) and irregular moons of giant planets (Kiss et al., 2016; Farkas-Takács et al., 2017). These observations provided continuous light curves which had significantly longer time-spans (up to 80 d) than ground-based measurements and therefore could break the ambiguity of rotational periods caused by daily aliases.

In this paper we report on observations of ten Centaurs: (250112) 2002 KY$_{14}$, (353222) 2009 YD$_7$, 2010 GX$_{34}$, 2010 JJ$_{124}$, (499522) 2010 PL$_{66}$, (463368) 2012 VU$_{85}$, (471931) 2013 PH$_{44}$, (472760) 2015 FZ$_{117}$, (514312) 2016 AE$_{193}$, and (523798) 2017 CX$_{33}$,[1] observed with *Kepler* in the K2 campaigns. One target, (250112) 2002 KY$_{14}$, has previous light curve measurements, and for this target we provide an updated, more accurate rotation period and light curve. The other nine Centaurs have no light curve measurements reported in the literature. Due to poorly constrained light curve properties for four targets we add reliable measurements for five objects to the group of Centaurs with known rotation periods and light curves. We also perform simple calculations to deduce whether the light curve variation of our targets can be caused more likely by shape effects or binarity.

2. Observations, data reduction and photometry

Kepler observed numerous Solar System objects during the K2 mission. The observing strategy and data reduction steps of centaurs have been analogous to other TNO and asteroid targets that we previously published (Pál et al., 2015a, 2015b; Kiss et al., 2016; Molnár et al., 2018). Since *Kepler* observed only selected pixels during each 60–80 d long Campaign, pixels over ~30 d long arcs of the apparent trajectories of the target were allocated for each Centaur (see Fig. 1 for an example).

---

[1] We use the provisional designations to identify our targets throughout the paper.

We processed the *Kepler* observations with the *fitsh* software package (Pál, 2012). First, we assembled the individual Target Pixel Files of both the track of the target and that of the nearby stars into mosaic images. Astrometric solutions were derived for every mosaic frame in the campaign, using the Full Frame Images (acquired once per campaign) as initial hints, and the individual frames were registered into the same reference system. We then enlarged the images by roughly 3 times, and transformed them into RA-Dec directions. This enlargement helped to decrease the fringing of the residual images in the next step, where we subtracted a median image from all frames. The median was created from a subset of frames that did not contain the target. We applied simple aperture photometry to the differential images based on the ephemeris provided by the JPL HORIZONS service.

We then discarded data points that were contaminated by the residuals of the stellar images, saturated columns and crosstalk patterns from the camera electronics – this is characterised by the duty cycle, the ratio of the number of frames used for the final light curve derivation and the total number of frames on which the target was theoretically visible. While this ratio is typically well above 50%, it is only ~34% for 2015 FZ1$_{17}$, which was very faint, and thus very sensitive to any structures in the background. We had to discard a large number of frames that were affected by stellar residuals, crosstalk patterns, or in which the object was not detected.

The light curves obtained were analysed with a residual minimization algorithm (Pál et al., 2016; Molnár et al., 2018). In this method we fit the data with a function $A + B \cos(2\pi f \Delta t) + C \sin(2\pi f \Delta t)$, where f is the trial frequency, $\Delta t = T - t$, T the approximate center of the time series, and A, B, and C are parameters to the determined. We search for the minimum in the dispersion curves for each frequency. As demonstrated in Molnár et al. (2018) the best fit frequencies obtained with this method are identical to the results of Lomb–Scargle periodogram or fast Fourier transform analyses, with a notably smaller general uncertainty in the residuals.

3. Results

3.1. Absolute magnitudes

We determined the absolute magnitudes of the targets, transformed from the K2 observations to the USNO B1.0 R-band photometric system (Monet et al., 2003), in the same way as in Pál et al. (2015a, 2015b). We calculated both the phase angle uncorrected (m_{11}^{R}) and phase angle corrected (m_{110}^{R}) absolute magnitudes. As the phase angle ranges of the observations were rather small (a maximum of $1°.7$ in the case of 2002 KY$_{14}$) we could not fit a phase angle correction curve when calculating m_{110}^{R}, but used a $\beta_R = 0.104 \pm 0.074$ mag deg^{-1} linear phase angle correction, obtained as the median values of the R-band correction factors of Centaurs in Ayala-Leora et al. (2018). While there is a specific

phase correction coefficient determined for 2002 KY$_{14}$, it is based on sparse and uncertain data (Alvarez-Candal et al., 2016), therefore we used the coefficient above even in this case. These absolute magnitudes are listed in Table 1 along with the basic observational parameters, using data from the Minor Planet Center.

3.2. Light curves

We were able to determine light curve periods from the periodograms for six targets. The folded light curves and residual dispersion plots are presented in Fig. 2, and the rotation periods and light curve amplitudes observed are summarized in Table 2.

In all cases we accepted the most prominent peak in the phase dispersion versus frequency plot as the actual primary light curve period. The quality of the light curve frequency/period determination is characterised by the accuracy of the frequency determination (converted to period uncertainty (h) in Table 2), and also by the ratio of the light curve peak over the r.m.s. of the phase dispersion at other frequencies. This latter was calculated for the whole frequency range investigated (S$_{f0}$ in Table 2) and also for a narrower frequency range of ± 1 d^{-1} around the peak (S$_{fp}$ in Table 2).

Period and amplitude uncertainties were also calculated with the *FAMIAS* and *Period04* methods using Fourier-transforms (Lenz and Breger, 2004; Zima, 2008). We calculated the formal least-squares uncertainties with both softwares, plus the Monte Carlo module of Period04 that generates sets of artificial data with randomized noise based on the residual light curve, and tries to fit them with the input frequency set. The latter method gave elevated uncertainties in three cases, most notably for 2012 VU$_{85}$ and 2013 PH$_{44}$, due to the low signal-to-noise ratio of the fitted frequency and the large scatter of data points. We also calculated the relative uncertainties for the main frequency components that generally agreed with the error estimates for the full amplitudes. We chose the larger of these estimates for each target (see the period and amplitude uncertainties in Table 2).

To characterise the possible double peak nature we folded the light curves with the double peak period and calculated the significance S$_{dp}$ of the difference between the two light curve halves (phases $0 \leq \phi < 0.5$ and $0.5 \leq \phi < 1$) following Pál et al. (2016, see eqs. 2, 3 and 4). These significance values were calculated for a series of bin numbers N = 16…24 which resulted in only slightly different S$_{dp}$ values for the same target. The actual mean S$_{dp}$-s are listed in Table 2. Following Pál et al. (2016) we used the criterion that for a detectable double peak behaviour S$_{dp} \geq 3$. In our sample only 2016 AE$_{193}$ has S$_{dp} = 1.8$, for all other targets S$_{dp} > 3$, indicating that a double peak light curve is likely in these latter cases.

3.3. Discussion of the individual targets

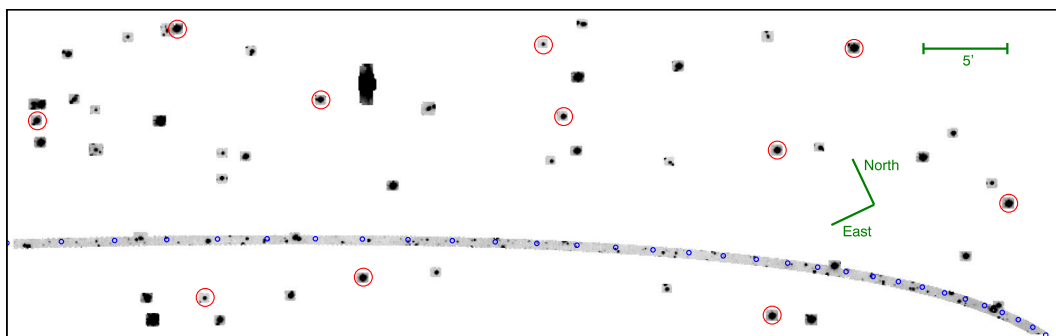(250112) 2002 KY$_{14}$ was discovered in 2002 by Trujillo, C. A. &

Fig. 1. The field-of-view of *Kepler* in which 2002 KY$_{14}$ was moving during the K2 Campaign 4, as an example. The stars involved in the determination of the absolute and differential astrometric solutions are indicated by red circles. The small blue circles indicate the position of the targets with a 1-day stepsize throughout the observations. The field is shown in the CCD frame, therefore the image is rotated with respect to the standard view. (For interpretation of the references to colour in this figure legend, the reader is referred to the web version of this article.)

Table 1

Summary of K2 light curve observations of our Centaur sample. The columns are: Name – provisional designation of the target; Cam. – K2 campaign number; Start – Start date of the K2 observations (Julian date); End – End date of the K2 observations (Julian date); Length – total length of the observations (day); Duty cycle – fraction of frames used for light curve photometry; r_h, Δ and α – heliocentric distance, target to observer distance and phase angle range during K2 measurements; m_{11}^R and m_{110}^R – phase angle uncorrected and corrected USNO B1.0 R-band absolute magnitude of the targets, derived from our K2 observations.

Name	Cam.	Start (JD)	End (JD)	Length (day)	#frame	Duty cycle	r_h (AU)	Δ (AU)	α (deg)	m_{11}^R (mag)	m_{110}^R (mag)
2002 KY$_{14}$	C04	2,457,061.7951	2,457,090.4838	28.689	1302	0.928	10.729... 10.774	9.931... 10.358	3.129... 4.837	9.85 ± 0.06	9.43 ± 0.10
2009 YD$_7$	C16	2,458,131.0852	2,458,150.7219	19.637	867	0.902	14.869... 14.906	14.474... 14.762	3.429... 3.788	10.13 ± 0.27	9.75 ± 0.27
2009 YD$_7$	C18	2,458,263.4745	2,458,302.3800	38.905	1401	0.734	15.125... 15.204	14.499... 15.169	3.086... 3.909		
2010 GX$_{14}$	C11	2,457,669.6537	2,457,679.5845	9.931	300	0.617	16.787... 16.791	16.349... 16.501	3.230... 3.400	8.48 ± 1.55	8.14 ± 1.56
2010 JJ$_{124}$	C11	2,457,682.7721	2,457,692.8663	10.094	395	0.800	23.994... 24.000	23.644... 23.814	2.320... 2.405	7.06 ± 0.75	6.81 ± 0.75
2010 PL$_{66}$	C12	2,457,754.3510	2,457,799.6318	45.281	1148	0.518	21.553... 21.616	21.042... 21.732	2.151... 2.591	8.25 ± 0.25	7.99 ± 0.25
2012 VU$_{85}$	C13	2,457,850.1437	2,457,880.8963	30.753	1022	0.679	15.583... 15.588	15.073... 15.577	3.148... 3.594	8.39 ± 0.44	8.16 ± 0.45
2013 PH$_{44}$	C12	2,457,756.1287	2,457,786.1048	29.976	859	0.586	24.735... 24.767	24.334... 24.813	2.078... 2.329	9.53 ± 0.21	9.17 ± 0.22
2015 FZ$_{117}$	C15	2,458,179.5332	2,458,246.4125	66.879	1108	0.338	14.694... 14.781	13.997... 14.956	2.507... 3.823	10.66 ± 0.47	10.24 ± 0.47
2016 AE$_{193}$	C16	2,458,122.4827	2,458,151.1715	28.689	1245	0.887	16.977... 16.996	16.508... 16.965	2.907... 3.339	8.64 ± 0.17	8.31 ± 0.17
2017 CX$_{33}$	C18	2,458,288.2605	2,458,298.2321	9.972	379	0.773	10.675... 10.685	10.377... 10.549	5.366... 5.537	11.33 ± 0.30	10.68 ± 0.30

Brown, M. E. Thirouin et al. (2010) reported on a single peak rotational period of 3.56 h or 4.2 ± 0.05 h with an amplitude of 0.13 ± 0.01 mag. Duffard et al. (2014) modeled the thermal emission of 2002 KY$_{14}$ using Herschel/PACS measurements of the "TNOs are Cool!" Open Time Key Program, using a NEATM model with fixed beaming parameter of $\eta = 1.2$, and obtained an effective diameter and albedo solution of D = 47^{+3}_{-4} km and $p_V = 5.7^{+1.1}_{-0.7}$%. Our new rotation period is P = 8.4996 ± 0.0036 h, with an asymmetric, double peak light curve. The amplitude of the first maximum is $\Delta m_1 = 0.090 \pm 0.009$ mag, with a secondary maximum of $\Delta m_2 = 0.028 \pm 0.008$ mag, i.e. the first peak is taller by 0.062 mag. The new spin period is the double period of the 4.2 h found by Thirouin et al. (2010).

(353222) 2009 YD$_7$ was observed in the K2 missions in two campaigns, C16 and C18 (see also Table 1). A well defined, double peak light curve is obtained with a period of P = 10.1590 ± 0.0008 h, and two similar light curve amplitude peaks of $\Delta m = 0.202 \pm 0.028$ mag and $\Delta m = 0.180 \pm 0.034$ mag.

For (463368) 2012 VU$_{85}$ we obtained a light curve with a period of P = 28.12 ± 1.66 h and light curve amplitude of $\Delta m = 0.38 \pm 0.05$ mag, assuming a single peak light curve. If the double peak light curve is considered (P = 56.2 h), it is the Centaur with the longest rotation period ever observed. The double peak period seems to be more likely due to the different first and second peaks observed in the double peak light curve ($S_{dp} = 3.2$).

A single peak light curve of (471931) 2013 PH$_{44}$ is detected with a period of P = 11.08 ± 0.12 h, and light curve amplitude of $\Delta m = 0.15 \pm 0.04$ mag. With the corresponding P = 22.16 ± 0.24 h double peak period the light curve is notably asymmetric, as presented in Fig. 2, making the double peak period more likely.

(514312) 2016 AE$_{193}$ has a single peak light curve with a period of P = 4.556 ± 0.013 h, and light curve amplitude of $\Delta m = 0.228 \pm 0.014$ mag. The double period light curve shows no significant asymmetry, and the light curve asymmetry parameter derived ($S_{dp} = 1.8$, see above) indicates that the light curve is rather single peak (a light curve folded with the double peak period is presented in Fig. 2 for consistency). However, this does not exclude that the double peak period is the rotation period of this target. E.g. a sufficiently symmetric triaxial ellipsoid – often used in simple asteroid shape modelling – produces a light curve with two identical half periods.

(523798) 2017 CX$_{33}$ is moving on a very high inclination orbit (see Table 2). It has a rotation period of P = 21.51 ± 0.13 h (double peak) with a light curve amplitude of $\Delta m = 0.27 \pm 0.11$ mag.

For four of our targets no unambiguous rotation period could be obtained ((499522) 2010 PL$_{66}$, 2010 GX$_{34}$, 2010 JJ$_{124}$, (472760) 2015 FZ$_{117}$, see Fig. 3). For these objects we provide an upper limit on the light curve amplitude only (see Table 2). As seen in Fig. 3 the Fourier amplitude depends strongly on the spin rate – there is a significant increase towards smaller frequencies/longer light curve periods, i.e. a light curve could have been detected at higher frequencies with a smaller amplitude, and we more likely miss light curve periods if P $\geq$ 1 d for these targets.

Altogether we add one updated light curve (2002 KY$_{14}$), and five new ones to the list of Centaurs with known light curve properties, previously containing 20 targets (Peixinho et al., 2020).

3.4. Comparison with Centaurs with known light curves

The most recent review by Peixinho et al. (2020) lists light curve periods for 20 Centaurs including 2002 KY$_{14}$ ($\equiv$2007 UL$_{126}$), and we have considered this sample as a reference sample for a comparison with our targets. The targets included are: (2060) Chiron, (5145) Pholus, (7066) Nessus, (8405) Asbolus, (10199) Chariklo, (31824) Elatus, (32532) Thereus, (42355) Typhon, (52872) Okyrhoe, (55567) Amycus, (60558) Echeclus, (65489) Ceto, (83982) Crantor, (95626) 2002 GZ$_{32}$, (120061) 2003 CO$_1$, (136204) 2003 WL$_7$, (145486) 2005 UJ$_{438}$, (281371) 2008 FC$_{76}$. We used the preferred single peak or double peak light curve periods as rotation periods as given in Peixinho et al. (2020), counter checked with the original papers (see the references in Peixinho et al., 2020). Note that the period of 8.32 h for 2005 UJ$_{438}$ is the double peak period according to Thirouin et al. (2010), and that for Ceto and Typhon the light curves periods used here are not the binary orbital periods, as discussed in Section 1.

We compare the rotation periods of the Centaurs in the reference sample with our targets in Fig. 4. Our targets are presented in this plot with their preferred single or double peak periods, as discussed in Section 3.2 above.

Using the rotation periods as presented in Fig. 4 the Centaurs with the three longest rotation periods are from our sample (2017 CX$_{33}$, 2013
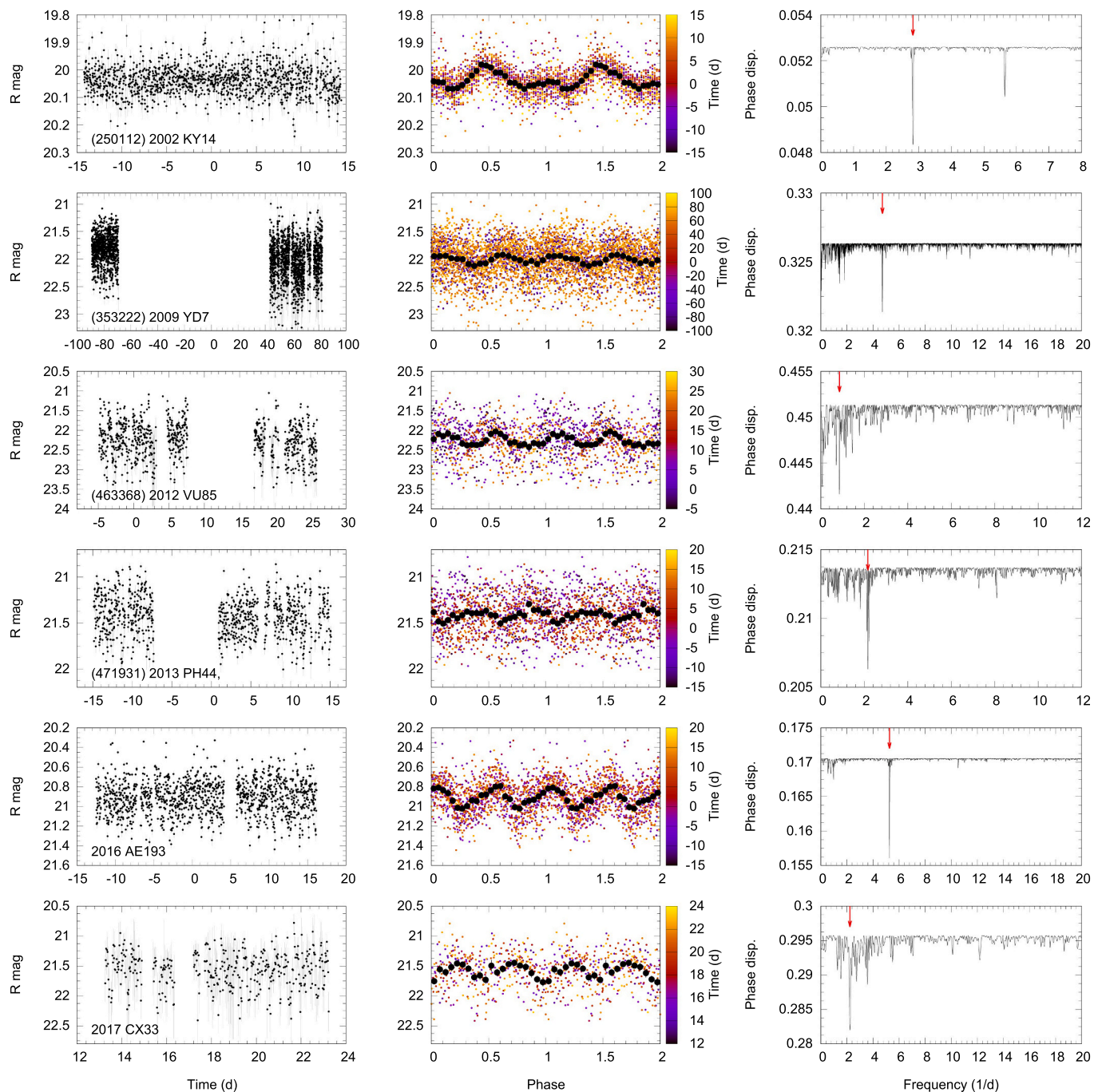
Fig. 2. The observed light curve (left), the phase curve (middle), in all cases folded with the most probable period (middle), and the residual dispersion versus frequency plot (left). In the middle column the colour scale represents dates, BJD-t_0, as indicated at the side of the figures. In the normalised residual plots red arrows mark the primary periods detected. (For interpretation of the references to colour in this figure legend, the reader is referred to the web version of this article.)

PH$_{44}$, 2012 VU$_{85}$). When considering double peak periods for all targets, however, there are several other objects with similar rotation periods (Typhon, Crantor, Amycus, Echeclus, Elatus). The single important feature is the quite long, P = 56.20 h rotation period of 2012 VU$_{85}$, not seen previously among Centaurs. Using the whole Centaur sample the mean rotation period is $\langle P \rangle$ = 9.2 h (8.9 h without our targets), which is now between the mean rotation period of the cold classicals (9.48 ± 1.53 h) and the rest of the TNOs (8.45 ± 0.58 h), as obtained by Thirouin and Sheppard (2019). The TNO sample in the Light Curve Database (LCDB Warner et al., 2009) has a spin rate distribution rather similar to that of Centaurs (red curve in Fig. 5), with a median rotation period of $\langle P \rangle$ = 8.84 h. A Maxwellian fit to the spin rate distribution (see e.g.

Pravec and Harris, 2000, for a discussion) seems to be an acceptable model as it provides a reduced-χ^2 value of $\lesssim 1$, using the square root of the number of objects in the specific bins as uncertainties.

4. Rotating elongated bodies versus binarity

4.1. Density estimates from Jacobi ellipsoid models

Leone et al. (1984) and Sheppard and Jewitt (2004) identified three main zones on the light curve amplitude versus rotational frequency plane (see Fig. 6), re-evaluated by Thirouin et al. (2010) and Benecchi and Sheppard (2013). Light curve variations of objects with small

Table 2
Summary of the derived rotation periods and amplitudes. $\langle R \rangle$ is the mean USNO B1.0 R-band brightness of the target. We list both the single peak and double peak periods (P_s and P_d, respectively), the one marked with bold-face characters is the more likely one according to our criteria. S_{f0} and S_{fp} are the significances of the light curve period determination, and S_{dp} is the significance parameter describing the possible double peak behaviour (see text for details). The amplitude upper limits are determined for possible periods shorter than 24 h. The last four columns list the main orbital parameters.

| Name	$\langle R \rangle$ (mag)	P_s (h)	P_d (h)	Δm (mag)	$\delta\Delta m$ (mag)	S_{f0}	S_{fp}	S_{dp}	a [au]	q [au]	e	i [°]
2002 KY$_{14}$	20.04	–	8.4996 ± 0.0036	0.0899	0.006	16.6	9.6	9.4	12.43	8.60	0.313	19.5
2009 YD$_7$	21.82	5.0795 ± 0.0004	10.1590 ± 0.0008	0.21	0.020	20.7	14.2	4.2	121.96	13.38	0.890	30.81
2010 GX$_{34}$	20.69	–	–	<0.6	–			–	29.01	16.57	0.429	11.54
2010 JJ$_{124}$	20.83	–	–	<0.5	–			–	85.55	23.61	0.724	37.70
2010 PL$_{66}$	21.56	–	–	<0.2	–			–	21.12	13.08	0.381	24.35
2012 VU$_{85}$	22.31	28.12 ± 1.66	56.24 ± 3.32	0.38	0.05	11.2	4.8	3.2	29.15	20.10	0.311	15.10
2013 PH$_{44}$	21.42	11.08 ± 0.12	22.16 ± 0.24	0.15	0.04	14.4	7.8	3.6	19.63	15.53	0.209	33.53
2016 AE$_{193}$	20.91	4.556 ± 0.013	9.112 ± 0.026	0.228	0.014	27.6	9.6	1.8	30.40	16.52	0.467	10.27
2015 FZ$_{117}$	22.31	–	–	<0.2	–	–	–	–	22.99	13.15	0.428	6.81
2017 CX$_{33}$	21.53	10.755 ± 0.064	21.51 ± 0.13	0.27	0.11	11.1	5.4	3.3	73.48	10.45	0.858	72.05
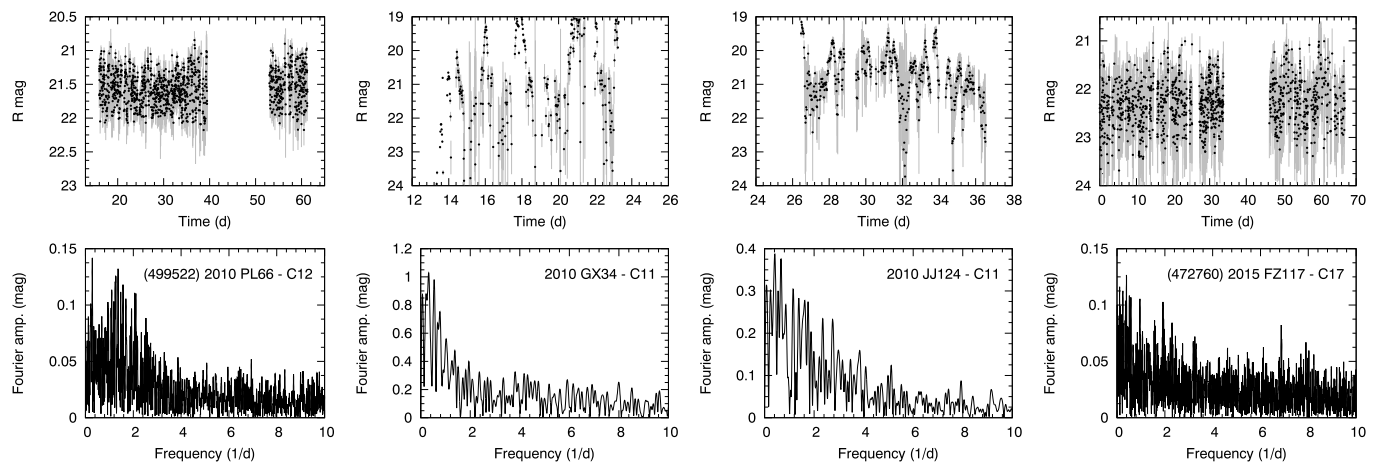
Fig. 3. The observed light curve (top row) and the corresponding Fourier amplitude plots (bottom row) of those three Centaurs (2010 PL$_{66}$, 2010 GX$_{34}$ and 2010 JJ$_{124}$) for which no rotation period could be obtained. Fourier amplitude plots are presented here instead of the dispersion residual plots as these were used to estimate the amplitude upper limits in the case of targets with no light curve period detected.
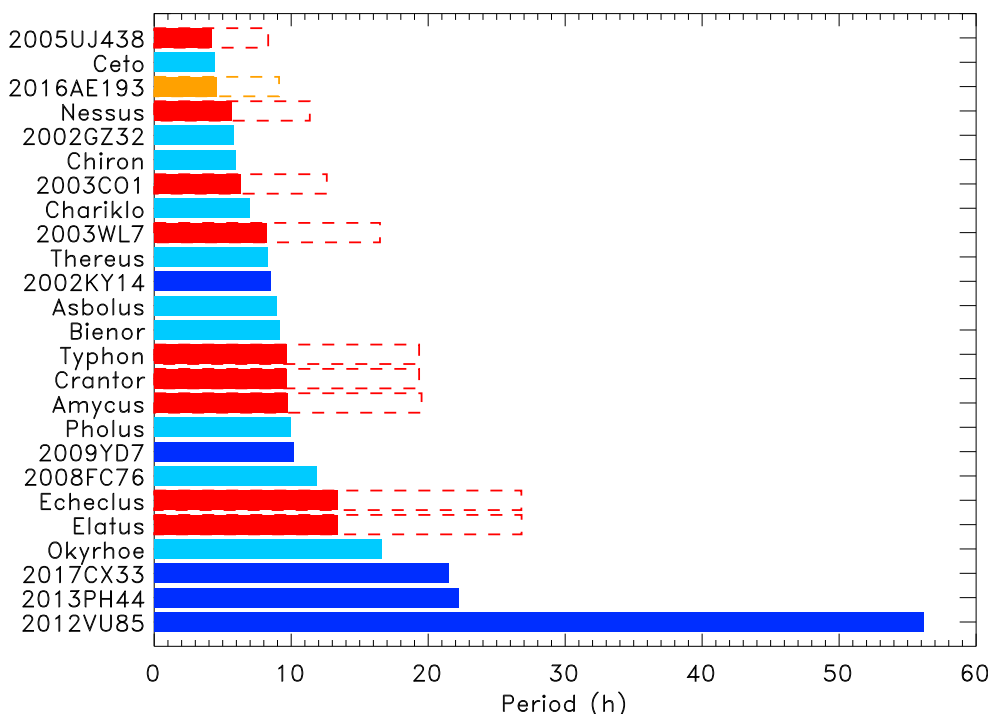

Fig. 4. Likely rotation periods of Centaurs in the literature and in our present work, sorted by increasing rotation period. The bar colours correspond to: red – literature, single peak period; orange – this study, single peak period; light blue – literature, double peak period; dark blue — this study, double peak period. In the case of single peak periods we also include the double peak periods with dashed lines. (For interpretation of the references to colour in this figure legend, the reader is referred to the web version of this article.)
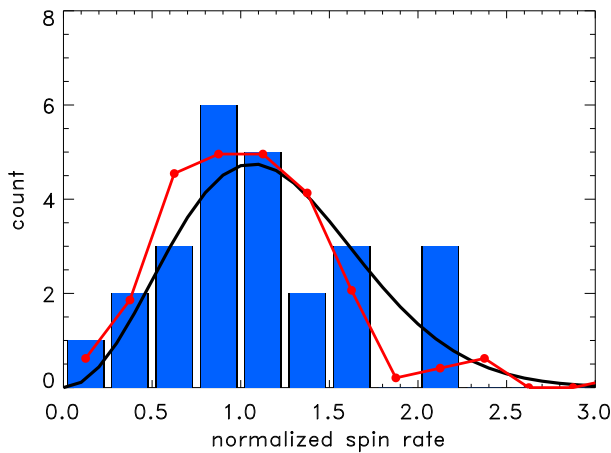
Fig. 5. Histogram presenting the spin rate distribution of Centaurs with our targets included, as a function of normalised spin rate (blue bars). The red curve represents the spin rate distribution of transneptunian objects as obtained from the LCDB, normalised to the total number of Centaurs in our sample. The black solid curve shows the Maxwellian fit to the Centaur data. (For interpretation of the references to colour in this figure legend, the reader is referred to the web version of this article.)

amplitudes ($\Delta m \leq 0.25$ mag or 0.15 mag) can either be caused by albedo and shape features or can as well be binaries (region A in Fig. 6). If the rotational equilibrium of a strengthless body is considered and approximated by a Jacobi ellipsoid, constant density curves can be drawn (blue dash-dotted curves in Fig. 6). We list the densities estimated this way for our targets in the last column of Table 3 following (see Eqs. (1) & (2) in 2007, and references therein), assuming $\vartheta = \pi/2$ aspect angle, i.e. equator-on viewing geometry and maximum light curve amplitude. Objects to the right of a curve of a constant density (e.g. 0.3 g cm^{-3} for Centaurs, region B) are likely rotating single bodies, if their rotational speed in below the breakup limit (4.0 cycle day^{-1} for 0.3 g cm^{-3}). The rotation of the objects to the left is too slow to cause elongation and a corresponding rotational light curve. For these objects the light curves are often explained by binarity (e.g. Leone et al., 1984; Sheppard and Jewitt, 2004).

For three of our targets the estimated Jacobi ellipsoid densities are in the order of ~0.5 g cm^{-3} ($\rho_{JE} = 0.54$, 0.39 and 0.48 g cm^{-3} for 2002

KY$_{14}$, 2009 YD$_7$ and 2016 AE$_{193}$, respectively, see Table 3), inside the range expected for smaller (D < 500 km) transneptunian objects and Centaurs (Grundy et al., 2019; Kiss et al., 2019). The Jacobi ellipsoid density estimates are, on the other hand, notably lower for 2012 VU$_{85}$, 2017 CX$_{33}$ and 2013 PH$_{44}$ ($\rho_{JE} < 0.1$ g cm^{-3}), outside the range of densities plausibly considered, indicating that the light curves in these cases cannot be explained by equilibrium figures of rotating strengthless bodies. As discussed above, objects in this part of the light curve amplitude vs. rotational frequency plot may be considered as binaries. However, due to the low amplitude ($\Delta m \leq 0.15$ mag) the light curves of 2002 KY$_{14}$ and 2013 PH$_{44}$ may as well be explained by albedo variegations on the surface, in addition to possible binarity or elongated shape. Also, the light curve amplitude of 2016 AE$_{193}$ is below the 0.25 mag limit originally considered for surface variegations.

4.2. Characterisation of potential binarity

It is a question in the case of a binary whether the observed rotation period is the common, synchronized period of a binary, or if we can see the light curve of a single body, rotating with an angular speed different from the orbital one. In the main belt small binary asteroids (D $\lesssim$ 10 km) are typically asynchronous if their rotation period is P $\lesssim$ 8 h (Pravec and Harris, 2007). Synchronous binaries are found for P $\geq$ 8 h, usually at the D $\approx$ 10 km sizes, but there are synchronous systems with D $\approx$ 100 km as well ((90) Antiope and (617) Patroclus-Menoetius), bracketing the size range of the Centaurs in our sample. Large asteroids (D $\geq$ 100 km) with small satellites also typically rotate faster (P $\lesssim$ 8 h Pravec and Harris, 2007).

In the plutino population, a likely parent population of Centaurs, Thirouin and Sheppard (2018) estimated that the incidence rate of contact binaries could be as high as ~50%. In the transneptunian region there is an overabundance of nearly equal-brightness (and therefore probably nearly equal-mass) binaries among the resolvable systems (Noll et al., 2008), and a large fraction, even close to 100% among cold classical Kuiper belt objects (Noll et al., 2014; Fraser et al., 2017).

While we cannot unambiguously identify a binary system from the light curve and rotation period alone, a simple check can be performed to show whether a specific system could potentially be a binary based on its light curve period and absolute magnitude. To characterise a system in this way we use the estimated 'separation', a_{bin}, the semi-major axis of the orbit of the potential binary. We assume that the binary has two equally sized and equal mass components (Noll et al., 2008). In the case
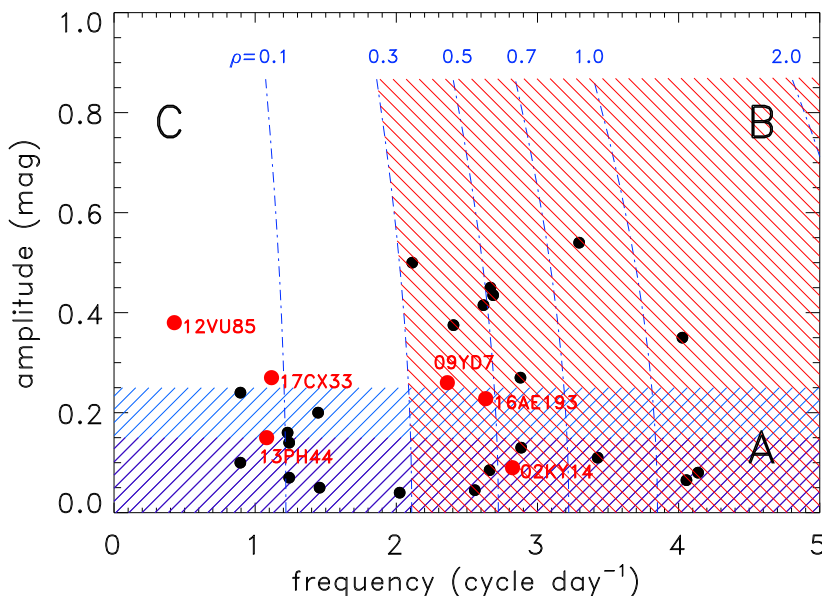

Fig. 6. Light curve amplitude versus frequency of the reference sample Centaurs (black dots) and our six targets (red dots). Blue dash-dotted curves represent the rotational frequencies and light curve amplitudes corresponding to the rotation of a strengthless body, modeled as Jacobi ellipsoids, of a specific density. The densities of the curves are shown at the top in g cm^{-3} units. In the blue and purple shaded areas (below $\delta m \leq 0.25$ or 0.15 mag, region A) light curves can be explained either by albedo variegations, deformed shape or binarity. Targets in the red shaded area (region B), right of the $\rho = 0.3$ g cm^{-3} curve, could be elongated due to rotation. Objects in region C should have densities notably below $\rho = 0.3$ g cm^{-3} in order to be elongated from rotation, and can be considered as binary candidates (see the text for a detailed discussion). (For interpretation of the references to colour in this figure legend, the reader is referred to the web version of this article.)

Table 3

Estimated binary system mass, binary size, surface gravitational acceleration, binary orbit semi-major axis, tidal dissipation parameter, and circularization and despinning timescale for our targets (see the text for the details of the estimation). We also list the ratio of the estimated semi-major axis, a, to the maximum semi major axis (a_{max}) for which despinning of the components can be expected within the lifetime of Solar system, $4.5 \cdot 10^9$ yr. The semi-major axis of the binary orbit and the tidal dissipation timescales cannot be estimated for targets without a known rotation period (bottom lines). Note that the system mass estimated for a binary is a factor of $\sqrt{2}$ *smaller* than it would be for a single object. In the last column we list the estimated density assuming a single body with a shape of a Jacobi ellipsoid, considering the actual double peak light curve period and the observed light curve amplitude (also not obtained for targets without a known rotation period).

Target	Mass (kg)	R_0 (km)	g (cm s^{-2})	a (km)	Q'	τ_{circ} (yr)	τ_{spin} (yr)	ρ_{JE} (g cm^{-3})
2002 KY$_{14}$	2.7E+16	16.6	0.6	34.8	5.1E+07	2.0E+04	1.4E+05	0.540
2009 YD$_7$	1.7E+16	14.3	0.6	33.8	6.8E+07	5.9E+04	3.3E+05	0.388
2012 VU$_{85}$	1.5E+17	29.5	1.2	137.4	1.6E+07	1.1E+06	1.7E+06	0.018
2013 PH$_{44}$	3.8E+16	18.6	0.7	74.1	4.0E+07	1.0E+06	2.1E+06	0.088
2016 AE$_{193}$	1.2E+17	27.6	1.1	60.8	1.8E+07	9.9E+03	6.4E+04	0.480
2017 CX$_{33}$	4.4E+15	9.1	0.4	35.4	1.7E+08	3.8E+06	7.8E+06	0.094
2010 GX$_{34}$	1.6E+17	29.9	1.2	–	1.6E+07	–	–	–
2010 JJ$_{124}$	9.7E+17	54.8	2.1	–	4.6E+06	–	–	–
2010 PL$_{66}$	1.9E+17	31.7	1.2	–	1.4E+07	–	–	–
2015 FZ$_{117}$	8.0E+15	11.1	0.4	–	1.1E+08	–	–	–

of our Centaur reference sample we used the radiometric size estimates based either on Herschel/PACS (Duffard et al., 2014; Fornasier et al., 2013) or WISE (Mainzer et al., 2016) observations, whenever these were available; when radiometric size was not available we simply used the default size (or albedo and absolute magnitude) estimate in Peixinho et al. (2020), and used this value to calculate the binary diameters and volumes (see e.g. Vilenius et al., 2014). The binary separation, a_{bin} is obtained from Kepler's third law, assuming a density of 0.7 g cm^{-3} to obtain the mass, characteristic for 10–100 km-sized Kuiper belt bodies and Centaurs (see e.g. Grundy et al., 2019; Kiss et al., 2019, for a latest compilation of Kuiper belt densities). The densities estimated for Ceto-Phorcys ($\rho = 1.37^{+0.66}_{-0.32} g cm^{-3}$ Grundy et al., 2007) and Typhon-Echidna ($\rho = 0.44^{+0.44}_{-0.17} g cm^{-3}$ Grundy et al., 2008) are at the lower/upper extremes of the densities of ~100 km-sized objects, and therefore may not be representative for the whole population.

We present the rotational frequency (cycle day^{-1}) as a function of the estimated size in Fig. 7 (upper panel), and compare it with other Centaurs (black dots) and with the population of transneptunian objects (TNOs), the latter ones taken from the LCDB. As seen previously in the rotation period comparison, the rotational frequencies of our targets are typically lower than those of other Centaurs and TNOs.

We used the ratio of a_{bin} to the effective diameter D_0 of the two equally sized bodies to characterise the potential binarity (see Taylor and Margot, 2011, for a more complex tidal evolution analysis using this parameter). For having enough space for two bodies in such a system $a_{bin}/D_0 > 1$ has to be fulfilled ($a_{bin}/D_0 = 1$ corresponds to a contact binary). As shown in Fig. 7 $1 < a_{bin}/D_0 < 2$ for many slower rotating Centaurs, but there are no objects with $a_{bin}/D_0 \geq 2$ in the Centaur reference sample. Note that 'classical' binary systems with tidal locking do not appear in these plots, as their rotational/orbital periods are notably longer (several days) than the typical rotation periods observed from light curves. These known binary systems also have notably larger separations than that can be deduced for a typical light curve target. The same calculations were performed for our targets. Radiometric size estimate is available for 2002 KY$_{14}$ only (Duffard et al., 2014), in the other cases we used our calculated R-band absolute brightness (m^R_{110}), and assumed a specific colour to obtain the H$_V$ V-band absolute magnitude. The colour distribution of Centaurs is bimodal (e.g. Peixinho et al., 2012, 2015) and the two colour groups correspond to two different average albedos (Lacerda et al., 2014; Farkas-Takács et al., 2020). For our targets we have colour information for 2012 VU$_{85}$ and 2002 KY$_{14}$ (Tegler et al., 2016; Wong et al., 2019), but as mentioned above, 2002 KY$_{14}$ has a reliable size estimate from radiometry. For 2012 VU$_{85}$ Tegler et al. (2016) obtained V-R = 0.63 ± 0.04 mag, and with this colour 2012 VU$_{85}$ is in the 'bright-red' group identified by Lacerda et al. (2014) which has a mean albedo of p$_V$ = 0.16 ± 0.08. We used this value to obtain the effective diameter of 2012 VU$_{85}$ from the absolute magnitude. As we

have no colour information for the other four targets we used a mean V-R = 0.558 mag and p$_V$ = 0.088, obtained from the Centaur sample with known geometric albedos (Duffard et al., 2014; Farkas-Takács et al., 2020), averaged over the two colour groups. The lack of colour information introduces a V-R error of ~0.18 mag in the H$_V$ estimate (Peixinho et al., 2015).

Interestingly, three of our targets, 2013 PH$_{44}$ 2017 CX$_{33}$ and 2012 VU$_{85}$ have $a_{bin}/D_0 \geq 2$, exceeding the values of the slowest rotating Centaurs, and also our other three targets have $1 \lesssim a_{bin}/D_0 \lesssim 2$, in the same range as the slower rotating Centaurs. Based on this estimate our six targets with rotation periods might be considered as potential binaries concerning this parameter only. However, as discussed above, a distorted rotating body or albedo variegations may also be plausible explanations for 2002 KY$_{14}$, 2009 YD$_7$ and 2016 AE$_{193}$.

4.3. Tidal evolution timescales

The simple calculations above assumed that the observed light curve period were both the rotation period and the orbital period of the binary, i.e. the system was tidally locked. It is, however, an important question whether the rotation of the individual bodies could have been slowed down by tidal forces and synchronized to the orbital period. Tidal dissipation is governed by the internal structure and composition of the bodies, and is usually considered through the tidal dissipation factor Q (e.g. Goldreich and Soter, 1966). Q factors of the terrestrial planets and satellites are usually found to be in the $10 \leq Q \leq 500$ range, and for our calculations in the following we apply the generally accepted $Q = 100$. However, as it is discussed e.g. in Grundy et al. (2007), smaller objects require a correction to Q, since their rigidity can be large compared with their self gravity, leading to deformations smaller than expected in hydrodynamic equilibrium. Therefore we use a corrected tidal dissipation factor, Q', obtained as (same as eq. 4 in Grundy et al., 2007):

$$Q' = Q\left(1 + \frac{19\mu}{2g\rho R}\right) \tag{1}$$

where μ is the rigidity, g the gravitational acceleration on the surface, ρ the density and R the radius of the object. This correction is very significant for small bodies with relatively rigid interiors. E.g. Grundy et al. (2007) obtained $Q' = 300$–$3 \cdot 10^6$ using $Q = 100$ for the Ceto-Phorcys system, in which the two bodies were in the 100–200 km size range. For our small Centaurs this correction is even more significant. Assuming $\mu = 4 \cdot 10^9$ Pa rigidity (that of icy bodies, see e.g. Gladman et al., 1996) we obtain $Q' \approx 10^7$ for all of our targets (actual values are listed in Table 3).

One of the important timescales related to the tidal evolution of binary systems is the orbit circularization timescale that we estimate as (Noll et al., 2008):
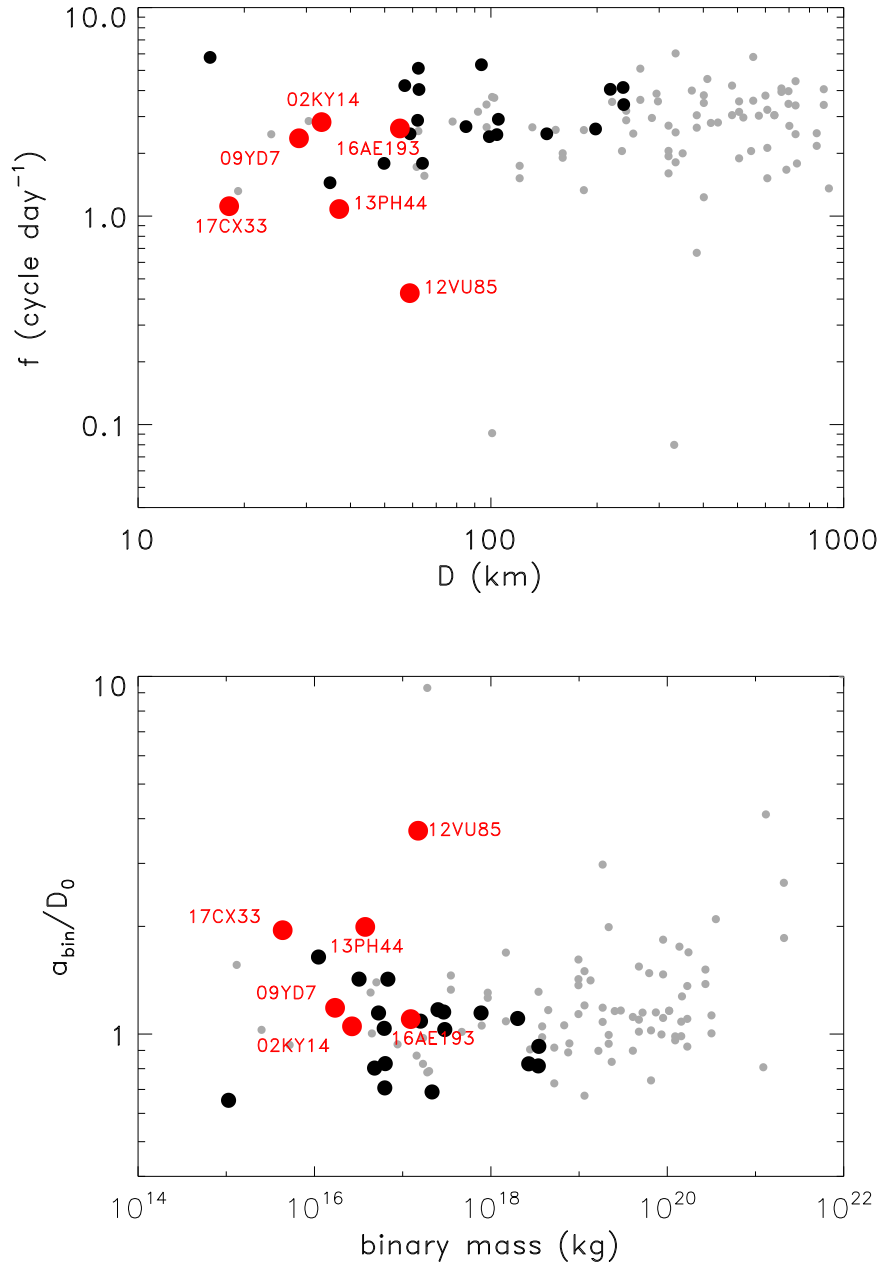
Fig. 7. Upper panel: Rotational frequency (cycle day^{-1}) versus the estimated diameter; Lower panel: a_{bin}/D_0 binary semi-major axis to size ratio versus the binary mass estimated. On both panels black and gray dots correspond to Centaurs from the reference sample and TNOs, respectively. Targets investigated in this paper are marked by red symbols. (For interpretation of the references to colour in this figure legend, the reader is referred to the web version of this article.)

$$\tau_{circ} = \frac{4Q'M_2}{63M_1}\left(\frac{a^3}{G(M_1+M_2)}\right)^{1/2}\left(\frac{a}{R_2}\right)^5 \qquad (2)$$

$$\tau_{spin} = \frac{Q'\Delta\omega_1 M_1 a^6}{GM_2^2 R_1^3} \qquad (3)$$

where a is the semi-major axis of the binary orbit, M is the mass, R is the radius of the body and G is the gravitational constant. The indices 1 and 2 refer to the primary and secondary, however, in our simple calculations all bodies are considered to be equal.

For our binary systems τ_{circ} obtained through these calculations are in the order of 10_4–10^6 yr, using the present estimated parameters of the systems, significantly smaller than the age of the Solar System. Another important question is whether in these systems the individual bodies could keep at least some of their own spin angular momentum and rotate with a period different from that of the binary orbit, or are fully spin locked due to tidal effects. We estimate this despinning (or spin-locking) timescale following (Grundy et al., 2007), as:

where $\Delta\omega_1$ is the change in angular speed with respect to the initial value. When the spin locking state is reached the mean motion n of the binary orbit is assumed to be equal to the angular speed obtained from the light curve period, i.e. $\Delta\omega_1 \approx \omega = n$. For our targets the despinning timescales are 10^5–10^7 yr, typically a few times longer than the corresponding circularization timescale. This suggests a fast tidal evolution for basically all systems, on timescales much smaller than the age of the Solar system (see also Table 3).

Kozai cycle tidal friction (Porter and Grundy, 2012) is a mechanism that can also create tight systems from an originally wider system with high eccentricity, if the inclination of the binary orbit to the heliocentric orbit is sufficiently large.

4.4. Encounters with giant planets

Tenuously bound binaries may be disrupted by giant planet encounters and Centaurs are especially susceptible in this respect. For our assumed system configurations, however, the ratio of the calculated binary orbit semi-major axis to the Hill radius is $a_{bin}/r_H \leq 0.0025$ for all our targets, while the Hill radii themselves are $r_H \leq 0.001$ AU. Encounters that close should be extremely rare (Noll et al., 2006). Concerning the target with the largest a_{bin} in our sample, Wlodarczyk et al. (2017) investigated the dynamics of 2012 VU$_{85}$, including close encounters with the giant planets Uranus and Neptune. According to their analysis this Centaur has no encounters with Uranus closer than ~4 AU, and with Neptune closer than ~1 AU. For 10% of the closest encounter distance with Neptune (0.1 AU) the gravitational influence distance of Neptune (Hill radius) would be ~10^4 km, significantly larger than the estimated ~140 km semi-major axis of the system, i.e. the binary system can be safely kept during these encounters (due to the similar mass and larger distances the encounters with Uranus are even safer).

5. Conclusions

We have presented Kepler Space Telescope light curve measurements of ten Centaurs, observed in the course of the K2 mission. We were able to derive rotation periods for six of these targets, of which five are new period determinations. Three of our six targets fall in the $P \geq 20$ h regime, not seen previously in ground based light curve period studies of Centaurs.

Due to the low amplitudes the light curves of 2013 PH$_{44}$ and 2002 KY$_{14}$ can be explained either by albedo variegations, binarity or elongated shape. 2009 YD$_7$ and 2016 AE$_{193}$ are just above the amplitude limit and have relatively short rotation periods indicating that their light curves could be caused by elongated shape. Due to their slow rotations and higher light curve amplitudes 2017 CX$_{33}$ and 2012 VU$_{85}$ are the most promising binary candidates.

Due to the lack of suitable spatial resolution by the current astronomical instrumentation binary systems in the typical distances of Centaurs cannot be discovered by direct imaging, but light curves with long rotation periods may be an indication for such systems. As shown for Centaurs in this paper and also previously for other small body populations (e.g. Szabó et al., 2017; Molnár et al., 2018) long, uninterrupted time series photometry is usually necessary to fully characterise such systems. The K2 mission of the *Kepler* was an excellent tool for these kind of studies (see Barentsen et al., 2018, for a summary). Similar results are expected from the TESS mission for Solar system targets (Pál et al., 2018).

References

Alvarez-Candal, A., Pinilla-Alonso, N., Ortiz, J.-L., Duffard, R., Morales, N., Santos-Sanz, P., A. Thirouin, A., J. S. Silva, J.S., 2016, Absolute magnitudes and phase coefficients of trans-Neptunian objects, Astronomy & Astrophysics, 586, A155.

Ayala-Leora, C., Alvarez-Candal, A., Ortiz, J.L., Duffard, R., Fernandez-Valenzuela, E., Santos-Sanz, P., Morales, N., 2018. Mon. Not. R. Astron. Soc. 481, 1848–1857.

Bailey, B.L., Malhotra, R., 2009. Two dynamical classes of Centaurs. Icarus 203 (1), 155–163.

Barentsen, G., Hedges, C., Saunders, N., et al., 2018. Kepler's Discoveries Will Continue: 21 Important Scientific Opportunities With Kepler & K2 Archive Data (White Paper, arXiv:1810.12554).

Benecchi, S.D., Sheppard, S.S., 2013. Light curves of 32 large transneptunian objects, The Astronomical Journal, Volume 145. Issue 5, article id 124.

Benecchi, S.D., Lisse, C.M., Ryan, E.L., Binzel, R.P., Schwamb, M.E., Young, L.A., Verbiscer, A.J., 2018. K2 precision lightcurve: twelve days in the Pluto-Charon system. Icarus 314, 265–273.

Berthier, J., Carry, B., Vachier, F., Eggl, S., Santerne, A., 2016. Prediction of transits of solar system objects in Kepler/K2 images: an extension of the virtual observatory service SkyBoT. Mon. Not. R. Astron. Soc. 458 (3), 3394–3398.

Davis, D.R., Farinella, P., 1997. Collisional evolution of Edgeworth-Kuiper belt objects. Icarus 125 (1), 50–60.

Di Sisto, R.P., Brunini, A., 2007. The origin and distribution of the Centaur population. Icarus 190 (1), 224–235.

Di Sisto, R.P., Brunini, A., de Elia, G.C., 2010, Dynamical evolution of escaped plutinos, another source of Centaurs, Astronomy and Astrophysics, Volume 519, id.A112, (7 pp).

Dotto, E.; Perna, D.; Barucci, M. A.; Rossi, A.; de Bergh, C.; Doressoundiram, A.; Fornasier, S., 2008, Rotational properties of centaurs and trans-neptunian objects. Lightcurves and densities, Astronomy and Astrophysics, Volume 490, Issue 2, 2008, pp.829–833.

Duffard, R., Ortiz, J.L., Thirouin, A., Santos-Sanz, P., Morales, N., 2009. 2009, transneptunian objects and Centaurs from light curves. Astron. Astrophys. 505 (3), 1283–1295.

Duffard, R.; Pinilla-Alonso, N.; Santos-Sanz, P.; Vilenius, E.; Ortiz, J. L.; Mueller, T.; Fornasier, S.; Lellouch, E.; Mommert, M.; Pal, A.; Kiss, C.; Mueller, M.; Stansberry, J.; Delsanti, A.; Peixinho, N.; Trilling, D. 2014, "TNOs are Cool": a survey of the transneptunian region. XI. A Herschel-PACS view of 16 Centaurs, Astron. Astrophys., Volume 564, id.A92, (17 pp).

Elliot, J.L., Kern, S.D., Clancy, K.B., Gulbis, A.A.S., Millis, R.L., Buie, M.W., Wasserman, L.H., Chiang, E.I., Jordan, A.B., Trilling, D.E., Meech, K.J., 2005. The deep ecliptic survey: a search for Kuiper belt objects and centaurs. II. Dynamical classification, the Kuiper belt plane, and the core population. Astron. J. 129 (2), 1117–1162.

Farkas-Takács, A., Kiss, Cs., Pál, A., Molnár, L., Szabó, Gy.M., Hanyecz, O., Sárneczky, K., Szabó, R., Marton, G., Mommert, M., Szakáts, R., Müller, T., Kiss, L.L., 2017. Properties of the irregular satellite system around Uranus inferred from K2, Herschel, and Spitzer observations. Astron. J. 154 (3), 119 (13 pp).

Fornasier, S.; Lellouch, E.; Müller, T.; Santos-Sanz, P.; Panuzzo, P.; Kiss, C.; Lim, T.; Mommert, M.; Bockelée-Morvan, D.; Vilenius, E.; Stansberry, J.; Tozzi, G. P.; Mottola, S.; Delsanti, A.; Crovisier, J.; Duffard, R.; Henry, F.; Lacerda, P.; Barucci, A.; Gicquel, A., 2013, TNOs are Cool: a survey of the trans-Neptunian region. VIII. Combined Herschel PACS and SPIRE observations of nine bright targets at 70-500 μm, Astronomy and Astrophysics, Volume 555, id.A15, (22 pp).

Fraser, Wesley C.; Bannister, Michele T.; Pike, Rosemary E.; Marsset, Michael; Schwamb, Megan E.; Kavelaars, J. J.; Lacerda, Pedro; Nesvorný, David; Volk, Kathryn; Delsanti, Audrey; Benecchi, Susan; Lehner, Matthew J.; Noll, Keith; Gladman, Brett; Petit, Jean-Marc; Gwyn, Stephen; Chen, Ying-Tung; Wang, Shiang-Yu; Alexandersen, Mike; Burdullis, Todd Sheppard, Scott; Trujillo, Chad, 2017, All planetesimals born near the Kuiper belt formed as binaries, Nature Astronomy, Volume 1, id. 0088.

Farkas-Takács, A., Kiss, Cs, Vilenius, E., Marton, G., Müller, T.G., Mommert, M., Stansberry, J., Lellouch, E., Lacerda, P., Pál, A., 2020. TNOs are Cool! A survey of the transneptunian region XV. Physical characteristics of 23 resonant transneptunian and scattered disk objects. Astron. Astrophys. accepted, arXiv: 2002.12712.

Gladman, Brett, Quinn, D.Dane, Nicholson, Philip, Rand, Richard, 1996. Synchronous locking of tidally evolving satellites. Icarus 122, 166–192.

Gladman, B., Marsden, B.G., VanLaerhoven, C., 2008. Nomenclature in the outer solar system. In: The Solar System Beyond Neptune. University of Arizona Press.

Goldreich, P., Soter, S., 1966. Q in the solar system. Icarus 5 (1), 375–389.

Grundy, W.M., Stansberry, J.A., Noll, K.S., Stephens, D.C., Trilling, D.E., Kern, S.D., Spencer, J.R., Cruikshank, D.P., Levison, H.F., 2007. The orbit, mass, size, albedo, and density of (65489) Ceto/Phorcys: a tidally-evolved binary Centaur. Icarus 191 (1), 286–297.

Grundy, W.M., Noll, K.S., Virtanen, J., Muinonen, K., Kern, S.D., Stephens, D.C., Stansberry, J.A., Levison, H.F., Spencer, J.R., 2008. (42355) Typhon Echidna: scheduling observations for binary orbit determination. Icarus 197 (1), 260–268.

Grundy, W.M., Noll, K.S., Buie, M.W., Benecchi, S.D., Ragozzine, D., Roe, H.G., 2019. The mutual orbit, mass, and density of transneptunian binary G!kún∥'hòmdímà (229762 2007 UK$_{126}$). Icarus 334, 30. https://doi.org/10.1016/j.icarus.2018.12.037.

Howell, Steve B., Sobeck, Charlie, Haas, Michael, Still, Martin, Barclay, Thomas, Mullally, Fergal, Troeltzsch, John, Aigrain, Suzanne, Bryson, Stephen T., Caldwell, Doug, Chaplin, William J., Cochran, William D., Huber, Daniel, Marcy, Geoffrey W., Miglio, Andrea, Najita, Joan R., Smith, Marcie, Twicken, J.D., Fortney, Jonathan J., 2014. The K2 mission: characterization and early results. Publ. Astron. Soc. Pac. 126 (938), 398.

Hromakina, T., Perna, D., Belskaya, I., Dotto, E., Rossi, A., Bisi, F., 2018. Photometric observations of nine transneptunian objects and Centaurs. Mon. Not. R. Astron. Soc. 474 (2), 2536–2543.

Kiss, C., Pál, A., Farkas-Takács, A.I., Szabó, G.M., Szabó, R., Kiss, L.L., Molnár, L., Sárneczky, K., Müller, T.G., Mommert, M., Stansberry, J., 2016. Nereid from space: rotation, size and shape analysis from K2, Herschel and Spitzer observations. Mon. Not. R. Astron. Soc. 457 (3), 2908–2917.

Kiss, Csaba, Marton, Gabor, Parker, Alex H., Grundy, Will, Farkas-Takacs, Aniko, Stansberry, John, Pal, Andras, Muller, Thomas, Noll, Keith S., Schwamb, Megan E., Barr, Amy C., Young, Leslie A., Vinko, Jozsef, 2019. The mass and density of the dwarf planet (225088) 2007 OR$_{10}$. Icarus 334, 3.

Lacerda, P., Jewitt, D.C., 2007. Densities of solar system objects from their rotational light curves. Astron. J. 133 (4), 1393–1406.

Lacerda, P., McNeill, A., Peixino, N., 2014. The unusual Kuiper belt object 2003 SQ$_{317}$. Mon. Not. R. Astron. Soc. 437 (4), 3824–3831.

Lenz, Patrik, Breger, Michel, 2004. Period04: a software package to extract multiple frequencies from real data. In: Zverko, J., Ziznovsky, J., Adelman, S.J., Weiss, W.W. (Eds.), The A-Star Puzzle, Held in Poprad, Slovakia, July 8-13, 2004, IAU Symposium, No. 224. Cambridge University Press, Cambridge, UK, pp. 786–790, 2004.

Leone, G., Farinella, P., Paolicchi, P., Zappla, V., 1984. 1984, Equilibrium models of binary asteroids. Astron. Astrophys. 140 (2), 265–272.

Lineweaver, C. H., Norman, M., 2017, eprint arXiv:1004.1091.

Mainzer, A.K., Bauer, J.M., Cutri, R.M., Grav, T., Kramer, E.A., Masiero, J.R., Nugent, C. R., Sonnett, S.M., Stevenson, R.A., Wright, E.L., 2016. NEOWISE Diameters and Albedos V1.0. EAR-A-COMPIL-5-NEOWISEDIAM-V1.0. NASA Planetary Data System.

Margot, J.-L., Pravec, P., Taylor, P., Carry, B., Jacobson, S., 2015. Asteroid systems: binaries, triples, and pairs. In: Michel, P., et al. (Eds.), Asteroids IV. Univ. of Arizona, Tucson, pp. 355–374.

Molnár, L., Pál, A., Sárneczky, K., Szabó, R., Vinkó, J., Szabó, Gy.M., Kiss, Cs., Hanyecz, O., Marton, G., Kiss, L.L., et al., 2018. Main-belt asteroids in the K2 Uranus field. Astrophys. J. Suppl. Ser. 234 (2), 37 (10 pp).

Monet, David G., Levine, Stephen E., Canzian, Blaise, Ables, Harold D., Bird, Alan R., Dahn, Conard C., Guetter, Harry H., Harris, Hugh C., Henden, Arne A., Leggett, Sandy K., Levison, Harold F., Luginbuhl, Christian B., Martini, Joan, Monet, Alice K.B., Munn, Jeffrey A., Pier, Jeffrey R., Rhodes, Albert R., Riepe, Betty, Sell, Stephen, Stone, Ronald C., Vrba, Frederick J., Walker, Richard L., Westerhout, Gart, Brucato, Robert J., Reid, I. Neill, Schoening, William, Hartley, M., Read, M.A., Tritton, S.B., 2003. The USNO-B catalog. Astron. J. 125 (2), 984–993.

Moore, Jeffrey M., McKinnon, William B., Cruikshank, Dale P., Gladstone, G. Randall, Spencer, John R., Stern, S. Alan, Weaver, Harold A., Singer, Kelsi N., Showalter, Mark R., Grundy, William M., Beyer, Ross A., White, Oliver L., Binzel, Richard P., Buie, Marc W., Buratti, Bonnie J., Cheng, Andrew F., Howett, Carly, Olkin, Cathy B., Parker, Alex H., Porter, Simon B., Schenk, Paul M., Throop, Henry B., Verbiscer, Anne J., Young, Leslie A., Benecchi, Susan D., Bray, Veronica J., Chavez, Carrie L., Dhingra, Rajani D., Howard, Alan D., Lauer, Tod R., Lisse, C.M., Robbins, Stuart J., Runyon, Kirby D., Umurhan, Orkan M., 2018. Great expectations: plans and predictions for New Horizons encounter with Kuiper belt object 2014 MU$_{69}$ ("Ultima Thule"). Geophys. Res. Lett. 45 (16), 8111–8120.

Noll, K.S., Levison, H.F., Grundy, W.M., Stephens, D.C., 2006. Discovery of a binary centaur. Icarus 184 (2), 611–618.

Noll, K.S., Grundy, W.M., Chiang, E.-I., Margot, J.-L., Kern, S.D., 2008. Binaries in the Kuiper belt. In: The Solar System Beyond Neptune. University of Arizona Press.

Noll, Keith S., Parker, Alex H., Grundy, William M., 2014. All Bright Cold Classical KBOs are Binary, American Astronomical Society. DPS meeting #46, id 507, 05.

Ortiz, J.L., Gutiérrez, P.J., Casanova, V., Sota, A., 2003. A study of short term rotational variability in TNOs and Centaurs from Sierra Nevada Observatory. Astron. Astrophys. 407, 1149–1155.

Pál, A., 2012. FITSH – a software package for image processing. Mon. Not. R. Astron. Soc. 421 (3), 1825–1837.

Pál, A., Szabó, R., Szabó, Gy.M., Kiss, L.L., Molnár, L., Sárneczky, K., Kiss, Cs, 2015a. Pushing the limits: K2 observations of the trans-neptunian objects 2002 GV$_{31}$ and (278361) 2007 JJ$_{43}$. The Astrophysical Journal Letters 804 (2), L45 (5 pp).

Pál, A.; Kiss, Cs., Horner, J., Szakáts, R.; Vilenius, E.; Müller, Th. G.; Acosta-Pulido, J.; Licandro, J.; Cabrera-Lavers, A.; Sárneczky, K.; Szabó, Gy. M.; Thirouin, A.; Sipöcz, B.; Dózsa, Á.; Duffard, R., 2015b, Physical properties of the extreme Centaur and super-comet candidate 2013 AZ$_{60}$, Astron. Astrophys., Volume 583, id.A93, (8 pp).

Pál, A., Kiss, C., Müller, T.G., Molnár, L., Szabó, R., Szabó, G.M., Sárneczky, K., Kiss, L.L., 2016. Large size and slow rotation of the trans-neptunian object (225088) 2007 OR$_{10}$ discovered from Herschel and K2 observations. Astron. J. 151 (5), 117 (8 pp).

Pál, A., Molnár, L., Kiss, Cs, 2018. TESS in the Solar System, Publications of the Astronomical Society of the Pacific, 130 (993), 114503.

Peixinho, N., Delsanti, A., Guilbert-Lepoutre, A., Gafeira, R., Lacerda, P., 2012, The bimodal colors of Centaurs and small Kuiper belt objects, Astron. Astrophys., Volume 546, id.A86, (12 pp).

Peixinho, N., Delsanti, A., Doressoundiram, A., 2015, Reanalyzing the visible colors of centaurs and KBOs: what is there and what we might be missing, Astron. Astrophys., Volume 577, id.A35, (16 pp).

Peixinho, Nuno, Thirouin, Audrey, Tegler, Stephen C., Di, Sisto, Romina, P., Delsanti, Audrey, Guilbert-Lepoutre, Aurélie, Bauer, James G., 2020. From Centaurs to comets – 40 years. In: Prialnik, D., Barucci, M.A., Young, L. (Eds.), The Transneptunian Solar System. Elsevier, pp. 307–329.

Porter, S.B., Grundy, W.M., 2012. KCTF evolution of trans-neptunian binaries: connecting formation to observation. Icarus 220 (2), 947–957.

Pravec, P., Harris, A.W., 2000. Fast and slow rotation of asteroids. Icarus 148, 12–20.

Pravec, P., Harris, A.W., 2007. Binary asteroid population. 1. Angular momentum content. Icarus 190 (1), 250–259.

Ryan, E.L., Sharkley, B.N.L., Woodward, C.E., 2017. Trojan steroids in the Kepler campaign 6 field. Astron. J. 153 (3), 116 (12 pp).

Sheppard, S.S., Jewitt, D.C., 2003. Earth Moon and Planets 92, 207.

Sheppard, S.S., Jewitt, D., 2004. Extreme Kuiper belt object 2001 QG$_{298}$ and the fraction of contact binaries. Astron. J. 127 (5), 3023–3033.

Szabó, R., Sárneczky, K., Szabó, Gy.M., Pál, A., Kiss, Cs.P., Csák, B., Illés, L., Rácz, G., Kiss, L.L., 2015. Main-belt asteroids in the K2 engineering field of view. Astron. J. 149 (3), 112 (5 pp).

Szabó, R.; Pál, A.; Sárneczky, K.; Szabó, Gy. M.; Molnár, L.; Kiss, L. L.; Hanyecz, O.; Plachy, E.; Kiss, Cs., 2016, Uninterrupted optical light curves of main-belt asteroids from the K2 mission, Astron. Astrophys., Volume 596, id.A40, (9 pp).

Szabó, Gy.M., Pál, A., Kiss, Cs., Kiss, L.L., Molnár, L., Hanyecz, O., Plachy, E., Sárneczky, K., Szabó, R., 2017. The heart of the swarm: K2 photometry and rotational characteristics of 56 Jovian Trojan asteroids, Astronomy and Astrophysics. Volume 599, id A44, 13.

Taylor, P.A., Margot, J.-L., 2011. Binary asteroid systems: tidal end states and estimates of material properties. Icarus 212, 661–676.

Tegler, S.C., Romanishin, W., Consolmagno, G.J., 2016. Two color populations of Kuiper belt and Centaur objects and the smaller orbital inclinations of red Centaur objects. Astron. J. 152 (6), 210 (13 pp).

Thirouin, A., Sheppard, S.S., 2018. The plutino population: an abundance of contact binaries. Astron. J. 155 (6), 248 (16 pp).

Thirouin, A., Sheppard, S.S., 2019. Light curves and rotational properties of the pristine cold classical Kuiper belt objects. Astron. J. 157 (6), 228 (19 pp).

Thirouin, A., Ortiz, J.L., Duffard, R., Santos-Sanz, P., Aceituno, F.J., Morales, N., 2010. Short-term variability of a sample of 29 trans-Neptunian objects and Centaurs, Astronomy and Astrophysics. Volume 522, id A93, 43.

Tiscareno, M.S., Malhotra, R., 2003. The dynamics of known Centaurs. Astron. J. 126 (6), 3122–3131.

Vilenius, E.; Kiss, C.; Müller, T.; Mommert, M.; Santos-Sanz, P.; Pál, A.; Stansberry, J.; Mueller, M.; Peixinho, N.; Lellouch, E.; Fornasier, S.; Delsanti, A.; Thirouin, A.; Ortiz, J. L.; Duffard, R.; Perna, D.; Henry, F., 2014, "TNOs are Cool": a survey of the trans-neptunian region. X. Analysis of classical Kuiper belt objects from Herschel and Spitzer observations, Astronomy & Astrophysics, Volume 564, id.A35, (18 pp).

Warner, B.D., Harris, A.W., Pravec, P., 2009. The asteroid lightcurve database. Icarus 202 (1), 134–146 updated on 2019 August 14, http://www.MinorPlanet.info/lightcurvedatabase.html.

Wlodarczyk, I., Cernis, K., Boyle, R.P., 2017. Discovery, orbit and orbital evolution of the distant object (463368) 2012 VU85. Acta Astronomica 67 (81).

Wong, Ian, Mishra, Aakash, Brown, Michael E., 2019. Photometry of active centaurs: colors of dormant active Centaur nuclei. Astron. J. 157 (6), 225 (11 pp).

Zima, W., 2008. FAMIAS - a userfriendly new software tool for the mode identification of photometric and spectroscopic times series. Communications in Asteroseismology 157, 387.